



# Thermal diffusivity from Fourier's inverse problem supervised by an optimization model: Theoretical analysis and experimental validation

Roberto Baccoli<sup>a,\*</sup>, Amit Kumar<sup>b</sup>, Anna Concas<sup>c</sup>, Gianluca Gatto<sup>b</sup>, Nicola Pintus<sup>a</sup>, Andrea Medda<sup>a</sup>, Giuseppe Rodriguez<sup>c</sup>

<sup>a</sup> Department of Civil, Environmental and Architectural Engineering, University of Cagliari, via Marengo 2, 09123 Cagliari, Italy

<sup>b</sup> Department of Electrical and Electronics Engineering, University of Cagliari, via Marengo 2, 09123 Cagliari, Italy

<sup>c</sup> Department of Mathematics and Computer Science, University of Cagliari, via Ospedale 72, 09124 Cagliari, Italy

## ARTICLE INFO

### Keywords:

Heat conduction  
Thermal diffusivity  
Inverse problem  
Optimization model

## ABSTRACT

An original experimental device coupled with an optimization technique, for determining the thermal diffusivity ( $\alpha_{\text{diff}}$ ) of solid materials, has been devised and experimentally validated. The inverse problem of the classical Fourier heat equation in transient condition is numerically supervised by an optimization procedure for the initial and boundary conditions from measurements. Imperfect adiabaticity on the insulated lateral surfaces is explained by modeling heat loss correction functions with additional time dependent Robin conditions. The optimization model identifies the optimal values of the heat transfer coefficients and of  $\alpha_{\text{diff}}$  by minimizing the residual function between the model predictions and the experimental data. Incorporating the heat loss corrections in the solution of the heat equation significantly improves the estimation of the  $\alpha_{\text{diff}}$ . Indeed, the time profile of the surface temperatures measured for a specimen of PPMA material is well reflected by the simulated curves. The estimated  $\alpha_{\text{diff}}$  is in good agreement with an experimental inter-comparison of eleven laboratories equipped with Laser Flash, hot disk, and hot bridge certified devices. Our results reveal a reliable capability of the model to identify the  $\alpha_{\text{diff}}$  value that explains the functional dependence underlying the experimental observations. The error lies in the range 5% or 34%, depending on whether the heat losses are accounted or not.

## 1. Introduction

The thermal characterization of a material becomes a fundamental target in those applications where the heat conduction is subject to specific requirements concerning the spatial distribution and time evolution of the temperature and of the heat flux.

The knowledge of the thermal properties becomes essential when the heat conduction has a critical bearing on the realistic estimation of the achievement and profitability of a given project, in terms of both energy saving, cost and operative requirements [1–5]. In this sense, nowadays it is a fundamental requirement the knowledge of the density and the specific heat to account for the transient evolution of the thermal power exchanges and, hence, of the thermal diffusivity as the parameter that governs the speed of heat diffusion in transient problems. The thermal diffusivity is a measure of the change in temperature induced by the heating

\* Corresponding author.

E-mail addresses: [rbaccoli@unica.it](mailto:rbaccoli@unica.it) (R. Baccoli), [amit.kumar@unica.it](mailto:amit.kumar@unica.it) (A. Kumar), [anna.concas@unica.it](mailto:anna.concas@unica.it) (A. Concas), [gatto@unica.it](mailto:gatto@unica.it) (G. Gatto), [nicola.pintus@unica.it](mailto:nicola.pintus@unica.it) (N. Pintus), [a.medda@unica.it](mailto:a.medda@unica.it) (A. Medda), [rodriguez@unica.it](mailto:rodriguez@unica.it) (G. Rodriguez).

<https://doi.org/10.1016/j.csite.2022.102533>

Received 17 May 2022; Received in revised form 14 October 2022; Accepted 29 October 2022

Available online 4 November 2022

2214-157X/© 2022 The Authors. Published by Elsevier Ltd. This is an open access article under the CC BY-NC-ND license (<http://creativecommons.org/licenses/by-nc-nd/4.0/>).

## Nomenclature

### Symbols

$a, b, c, d$	Geometrical coordinates of the specimen's edges [m]
$h_{c d}$	Surface heat transfer coefficient, between the surrounding environment and the lateral insulated surfaces of the specimen [ $\text{W}/\text{m}^2\text{K}$ ]
$J$	Jacobian operator
$m$	Number of time steps inside $T$
$n_1$	Number of space steps along the $x$ -coordinate of the spatial mesh
$n_2 - 2$	Number of space steps along the $y$ -coordinate of the spatial mesh
$p$	Spatial position covered by a generic point of the specimen
$\mathcal{P}$	3D spatial domain composed by the set of the geometrical point covered by the specimen
$T$	Temporal duration of the measurements [s]
$x, y, z$	Spatial coordinates [m]

### Greek symbols

$\alpha$	Thermal diffusivity [ $\text{m}^2/\text{s}$ ]
$\lambda$	Thermal conductivity [ $\text{W}/\text{mK}$ ]
$\vartheta(p, \tau)$ or $\vartheta(x, y, \tau)$	Spatial distribution of the temperature as a function of the time, numerically determined [K]
$\vartheta'(x_i, y_j, \tau)$	Experimental value of the temperature, measured for a position at $i$ th $x$ , $j$ th $y$ and at a generic instant $\tau$ [K]
$\tau$	Time [s]
$\Omega$	2D spatial domain composed by the set of the geometrical position covered by the point of the specimen in the $xy$ -plane

### Subscripts

$a$	Refers to a quantity related to the lateral surface of the specimen at $x = a$
$b$	Refers to a quantity related to the lateral surface of the specimen at $x = b$
$c$	Refers to a quantity related to the lateral surface of the specimen at $x = c$
$d$	Refers to a quantity related to the lateral surface of the specimen at $x = d$
$\ell$	Refers to a quantity recursively evaluated by the optimization model at step $\ell$ th
opt	Refers to an optimal value, numerically determined by the optimization model

source over the time, which can be reconstructed by solving the differential heat equation [6,7]. Determining the thermal diffusivity is a challenging task because it belongs to a class of inverse problems [8] for which the parameter to be estimated is very sensitive to the measured data required for its computation. Before going on with the description of our investigation, it is relevant to mention popular techniques and technologies that have been employed for determining the thermal diffusivity of a given material. Some examples are laser flashes [9], laser interferometers [10] and photothermal techniques [11,12], which however require relatively complex and quite expensive instrumentation [13,14]. The hot wire technique [15–17] is a standard transient solution and was specifically devised for liquids [18,19]. Subsequently, the technique was integrated for application to solid polymers [20,21]. Moreover, this technique exhibits a better sensitivity and it is reliable for thermal diffusivity determination [19,22]. The Hot Disk technique [23,24] is the most well-known, and it has also reached an appropriate commercial maturity. It is a contact technique based on the transient plane source method, that measures the response function of a hot sensor when it is arranged between two identical specimens. This procedure can be used for a variety of materials, but realizing a good thermal contact between the sensor and the two specimens is essential for an effective measurement. In recent studies, the problem of predicting thermal diffusion parameters was performed for diverse applications and by using different techniques. For example, in [25] simulated thermal images were used to predict thermal diffusion parameters during microwave heating procedure, in [26] coupling controlled environmental forcing and a transient plane source method were employed for building insulation material applications, and the Ångström method was used in [27] to measure the heat diffusivity for the vapor chambers and in [28] to numerically obtain the temperature distribution for the polymers.

Besides the above mentioned experimental techniques, there are also many mathematical strategies that have been implemented for modeling the response of measurement devices. Several mathematical schemes are based on inverse problem procedure [8,25,29–33] and consist of two fundamental steps. Firstly, the specific solution that arises from a priori and suitable initial and boundary conditions is analytically or numerically determined. Secondly, the derived solution is compared to the one experimentally acquired under the same conditions. These schemes are termed as direct solution methods [29,30,34]. They determine the values of the thermal transport properties for which the time evolution of the measured temperature optimally matches the heat conduction

solution for the prescribed boundary and initial conditions. Many models were developed for a finite or a semi-infinite geometry, where the theoretical aspects are reduced to a mono dimensional formalism. In these cases, the experimental apparatus should be arranged in order to realize an approximation of such symmetry [28]. Indeed, the accuracy of the optimal value of the estimated thermal diffusivity quantity is, in general, significantly affected by the deviation between the mathematical representation of the boundary and initial conditions, that are conceptually assumed a priori, and the physical realization of the correspondent conditions [35–37]. In a recent study [38], a multi-block lattice Boltzmann method was adopted to predict the thermal contact resistance at the interface of two solids. Moreover, in [39] the authors modeled heat transfer of an aluminum rod in a much-simplified experimental environments settings with finite domains using Green’s function techniques in three dimensions. Their work showed the utility of inversion method to simultaneously determine the thermal diffusivity and coefficient of thermal expansion for thermally conductive solid materials. Another kind of investigation was conducted in [40], where the authors studied the potential of an entangled porous metallic wire material as thermal insulation material employing numerical and experimental evaluation. The experimental results performed using laser thermal analyzer showed an increase in effective thermal conductivity of the metallic wire with increasing temperature. The numerical model results were found to be in good agreement with the experimental results. In [41] a partial differential system is converted into ordinary differential equations by using the transformations in order to characterize the thermal parameters in a fluid flow with variable conductivity and diffusivity. In addition to these techniques, in [42] it is proposed a low-cost Gaussian shape laser-spot step heating method to measure the thermal diffusivity for solids. Employing this technique, the authors showed that thermal diffusivity for materials ranging from good thermal conductors to thermal insulators, including thick and thin samples can be obtained with high accuracy and precision. In [43] the thermal performance of phase change materials (PCM) embedded with fins and metal foam is investigated. The theoretical model therein proposed reveals that the melting rate becomes higher as the ratio of thermal diffusivity increases among other parameters.

The overarching objective of the present investigation is to develop a low-cost yet simple to use method for estimating the effective thermal diffusivity of a solid material. The technique is based on an optimized direct solution method applied to a 3D regular geometry and make use of a low-cost apparatus in which the lateral surfaces of the specimen are kept insulated and the opposite largest sides are subjected to modulable heat sources for generating a suitable thermal field as the test of the specimen is in progress. The heat equation in transient condition is numerically solved, considering a 2D formalism by assuming a symmetric geometry. The model is refined and improved by modeling heat loss correction functions, to account for the uncertainty about the lack of a perfect adiabaticity on the insulated lateral surfaces. Therefore, heat transfer coefficients at lateral surfaces are introduced by additional suitable Robin conditions and are then subject to a globally optimization together with the value of the thermal diffusivity. Incorporating the heat loss correction functions, in the solution of the heat equation, significantly improves the estimation of the thermal diffusivity. The experimental apparatus, supervised by the optimization model, has been successfully tested on a PMMA specimen, which can be considered as a reference material since its thermal properties have been widely studied [44]. Moreover, the data on PMMA are available in the scientific literature since it is broadly employed in many applications of engineering [45,46]. Indeed, this material adequately fulfills the assumptions adopted in the present study for reducing the 3D to a 2D problem. In this case study, the experimental profile of the time evolution of the surface temperature is well reflected by the simulated curve generated by the model. The estimated values of the thermal diffusivity are compared with the current literature and with the measured values delivered by an experimental investigation [46] consisting of an inter laboratory comparison of eleven laboratories equipped with laser flash, hot disk and hot bridge certified devices. The obtained results are quite satisfactory, especially considering the low-cost equipment used in this study.

## 2. Geometry, initial and boundary conditions

Let us consider the rectangular cuboid domain representing the geometry of a given specimen

$$\mathcal{P} = \{p = (x, y, z) \in \mathbb{R}^3 : a \leq x \leq b, c \leq y \leq d, e \leq z \leq f\}.$$

The 6 faces of its closure surface will be denoted by  $\partial_a\mathcal{P}$ ,  $\partial_b\mathcal{P}$ ,  $\partial_c\mathcal{P}$ ,  $\partial_d\mathcal{P}$ ,  $\partial_e\mathcal{P}$ , and  $\partial_f\mathcal{P}$ , where

$$\partial_{a|b}\mathcal{P} = \{p = (x, y, z) \in \mathbb{R}^3 : x = a|b, c \leq y \leq d, e \leq z \leq f\},$$

$$\partial_{c|d}\mathcal{P} = \{p = (x, y, z) \in \mathbb{R}^3 : a \leq x \leq b, y = c|d, e \leq z \leq f\},$$

$$\partial_{e|f}\mathcal{P} = \{p = (x, y, z) \in \mathbb{R}^3 : a \leq x \leq b, c \leq y \leq d, z = e|f\}.$$

- the faces  $\partial_a\mathcal{P}$  and  $\partial_b\mathcal{P}$ , in contact with the two reservoirs of thermal energy, will be denoted respectively as the hot and the cold side;
- the rest of the boundary lateral surface  $\partial_c\mathcal{P}$ ,  $\partial_d\mathcal{P}$ ,  $\partial_e\mathcal{P}$ , and  $\partial_f\mathcal{P}$ , are surrounded by a guard section of insulating material.

Let us consider the 2D restriction of the domain  $\mathcal{P}$  by fixing  $z = e$ , that is

$$\Omega = \{p = (x, y) \in \mathbb{R}^2 : a \leq x \leq b, c \leq y \leq d\}.$$

The description of each face of  $\Omega$  is evident from the definition above.

Let  $\vartheta(P, \tau)$  designate the temperature at a given point  $P$  and at a given time  $\tau$ . The temperature when the specimen is in thermal equilibrium with the surrounding environment can be considered as representative of the initial condition. The expected solution  $\vartheta$  is subject to satisfy

$$\lim_{\tau \rightarrow 0^+} \vartheta(p, \tau) = \vartheta_0, \quad p \in \Omega, \tag{2.1}$$

where  $\vartheta_0$  represents the initial value of the temperature of the specimen.

Two kind of boundary conditions are considered:

- (a) the time evolution of the surface temperatures on the hot and the cold side of the specimen,  $\varphi_a(\tau)$  and  $\varphi_b(\tau)$ ;
- (b) the time evolution of the heat loss at the lateral surfaces  $\partial_{c,d}\Omega$ , for which the heat exchanged with the surrounding environment, according to Newton's law, is assumed to be a linear function of the temperature difference between the surfaces and the surrounding medium, that is,

$$-k \frac{\partial \vartheta}{\partial y} \Big|_{\partial_{c,d}\Omega} = h_{c|d} [\vartheta(p, \tau) - \vartheta_0], \quad p \in \partial_{c|d}\Omega, \tag{2.2}$$

where  $h_{c|d}$  denotes the combined or the effective heat transfer coefficients which simultaneously account for the convection and the radiation exchanges. More specifically,  $h_{c|d}$  denotes the coefficients  $|h_c|$  and  $|h_d|$  on the faces  $\partial_c\Omega$  and  $\partial_d\Omega$  respectively. The sign of these coefficients depends on the normal vector orientation on the faces.

We remark that the initial temperature  $\vartheta_0$  and the surface temperature  $\varphi_a(\tau)$  and  $\varphi_b(\tau)$ , are experimentally measured quantities.

Let  $k$  [W/mK] be the thermal conductivity of the substance that fills the reference infinitesimal volume,  $\rho$  [kg/m<sup>3</sup>] the density at point  $P$  of the specimen and  $c_p$  the specific heat at constant pressure. Let  $\alpha = \frac{k}{\rho c_p}$  designate the thermal diffusivity of the specimen under consideration. The following scheme summarizes the mathematical framework for estimating the thermal diffusivity of a given specimen

$$\begin{cases} \frac{1}{\alpha} \frac{\partial \vartheta(p, \tau)}{\partial \tau} = \Delta \vartheta(p, \tau), & p \in \Omega, \\ \lim_{\tau \rightarrow 0^+} \vartheta(p, \tau) = \vartheta_0, & p \in \Omega, \\ \vartheta(p, \tau) = \varphi_{a|b}(\tau), & p \in \partial_{a|b}\Omega, \\ \frac{\partial \vartheta}{\partial y} \Big|_{\partial_{c|d}\Omega} = \beta_{c|d} [\vartheta(p, \tau) - \vartheta_0], & p \in \partial_{c|d}\Omega, \end{cases} \tag{2.3}$$

where the parameter  $\beta_{c|d} = h_{c|d}/k$  represents the ratio between the heat transfer coefficient and the thermal conductivity on the boundary lateral surfaces  $\partial_{c|d}\Omega$ . We observe that in the first line of Eq. (2.3) we used the more common symbol  $\Delta$  instead of  $\nabla^2$  to denote the Laplace operator.

At this point, our aim is to estimate the parameters  $\alpha$  and  $h_{c|d}$ , by numerically solving Eq. (2.3), as shown in the following section.

### 3. Finite differences scheme and the inverse problem of the heat equation

Let us consider the two dimensional heat equation

$$\frac{1}{\alpha} \frac{\partial \vartheta(x, y, \tau)}{\partial \tau} = \frac{\partial^2 \vartheta(x, y, \tau)}{\partial x^2} + \frac{\partial^2 \vartheta(x, y, \tau)}{\partial y^2}, \tag{3.1}$$

with  $x \in [a, b]$ ,  $y \in [c, d]$  and  $\tau \geq 0$ . The considered boundary Dirichlet time depending conditions are given by

$$\vartheta(a, y, \tau) = \varphi_a(y, \tau), \quad \vartheta(b, y, \tau) = \varphi_b(y, \tau), \quad y \in [c, d], \tag{3.2}$$

while the Neumann boundary conditions are represented by the equations

$$\frac{\partial \vartheta(x, c, \tau)}{\partial y} = \beta_c [\vartheta(x, c, \tau) - \vartheta_0], \quad \frac{\partial \vartheta(x, d, \tau)}{\partial y} = \beta_d [\vartheta(x, d, \tau) - \vartheta_0], \tag{3.3}$$

for  $x \in [a, b]$  and where  $\beta_c = |h_c|/k$  and  $\beta_d = |h_d|/k$  are the ratio between the absolute value of the heat transfer coefficient and the thermal conductivity on the boundary lateral surfaces  $\partial_c\Omega$  and  $\partial_d\Omega$  respectively.

Let  $\vartheta(x_i, y_j, \tau_\mu) = \theta_{ij}^\mu$  and consider the mesh

$$\begin{aligned} x_i &= a + ir_x, & i &= 0, 1, \dots, n_1 + 1, \\ y_j &= c + jr_y, & j &= 0, 1, \dots, n_2 - 1, \end{aligned}$$

where  $r_x = \frac{b-a}{n_1+1}$  and  $r_y = \frac{d-c}{n_2-1}$  are the space steps and let  $r_\tau = \frac{T}{m}$  be the time step. Using a backward time, centered space finite differences method (implicit Euler), we obtain for  $\mu = 1, \dots, m$  the linear equation

$$\frac{1}{\alpha} \left( \frac{\theta_{i,j}^\mu - \theta_{i,j}^{\mu-1}}{r_\tau} \right) = \frac{\theta_{i-1,j}^\mu - 2\theta_{i,j}^\mu + \theta_{i+1,j}^\mu}{r_x^2} + \frac{\theta_{i,j-1}^\mu - 2\theta_{i,j}^\mu + \theta_{i,j+1}^\mu}{r_y^2} \tag{3.4}$$

that, by setting  $r_x^2 = r_y^2 = r^2$ , can be rewritten as the equation

$$-\theta_{i-1,j}^\mu - \theta_{i,j-1}^\mu + \left( \frac{1}{\alpha} \frac{r^2}{r_\tau} + 4 \right) \theta_{i,j}^\mu - \theta_{i,j+1}^\mu - \theta_{i+1,j}^\mu = \frac{1}{\alpha} \frac{r^2}{r_\tau} \theta_{i,j}^{\mu-1}. \tag{3.5}$$



where the additional subscript “ $\ell$ ” on symbols corresponds to an initial guess value and the last two terms in brackets are the columns of the Jacobian operator  $\mathcal{J}$  applied to the functions  $\theta_{c,d}$ .

The linearized least squares problem can be solved by the normal equation

$$\mathcal{J}(\theta_{c,d})^T \mathcal{J}(\theta_{c,d}) (\mathcal{P} - \mathcal{P}_\ell) = \mathcal{J}(\theta_{c,d})^T \left[ \theta'_{c,d} - \theta_{c,d}(\alpha_\ell, h_{c,\ell}, h_{d,\ell}) \right], \quad (3.12)$$

where

$$\mathcal{P}_\ell = \begin{bmatrix} \alpha_\ell \\ h_{c,\ell} \\ h_{d,\ell} \end{bmatrix}, \quad \mathcal{P} = \begin{bmatrix} \alpha \\ h_c \\ h_d \end{bmatrix}$$

denote the vectors of the optimization parameters.

From Eq. (3.12) we obtain the following iteration function:

$$\mathcal{P}_{\ell+1} = \mathcal{P}_\ell + \mathcal{M}(\theta_{c,d})^{-1} \mathcal{J}(\theta_{c,d})^T \left[ \theta'_{c,d} - \theta_{c,d}(\alpha_\ell, h_{c,\ell}, h_{d,\ell}) \right], \quad (3.13)$$

where  $\mathcal{M}(\theta_{c,d}) = \mathcal{J}(\theta_{c,d})^T \mathcal{J}(\theta_{c,d})$ . Since an explicit representation of the Jacobian of  $\theta_{c,d}$  is not available, an approximation of it by a finite difference scheme can be used to iteratively improve the initial guess in an attempt to converge to an optimal solution. The algorithm selects the search direction along which an improvement of the objective functions  $\psi(\alpha, h_c, h_d)$  might be obtained. At each iteration the solver updates the optimization parameters, considering their values inside a space for which the constraints are satisfied within the constraint tolerance value ( $\epsilon_1$ ). The algorithm uses two tolerances as possible stopping criteria:

- the step size tolerance ( $\epsilon_2$ ), is a lower bound on the size of a step, meaning the size of the change in location where the objective function is evaluated;
- the objective function tolerance ( $\epsilon_3$ ), is a lower bound on the change in the value of the objective function during a step.

If the solver attempts to adopt a step size that is smaller than the  $\epsilon_2$  tolerance or the improvement of the objective function, at a specific iteration, is smaller than the  $\epsilon_3$  tolerance, the iterations end.

If the constraints are satisfied to within the  $\epsilon_1$  tolerance, the accuracy of the detected solution, at the end of the iterations, is established by the so called first-order optimality measure. The first-order optimality measure is a measure of the gradient of the objective functions  $\psi(\alpha, h_c, h_d)$  and corresponds to infinity norm of  $\nabla(\psi(\alpha, h_c, h_d))$ ,

$$\left\| \nabla(\psi(\alpha, h_c, h_d)) \right\|_\infty = \max_i \nabla(\psi(\alpha, h_c, h_d))_i. \quad (3.14)$$

The analytical expression of the first order optimality measure should be zero in correspondence of the optimal values of the design parameters, namely:

$$\left\| \nabla(\psi(\alpha, h_c, h_d)) \right\|_\infty = 0. \quad (3.15)$$

However, the solver considers numerically satisfied this condition even to within a certain tolerance  $\epsilon_4$ . Therefore, the inequality

$$\left\| \nabla(\psi(\alpha, h_c, h_d)) \right\|_\infty < \epsilon_4, \quad (3.16)$$

is considered as a numerical approximation of the analytical expression of (3.15). The accuracy of the results obtained by the performed simulations is correlated to the following key tolerances values:

- constraint tolerance value ( $\epsilon_1 = 10^{-4}$ );
- step size tolerance ( $\epsilon_2 = 10^{-3}$ );
- objective function tolerance ( $\epsilon_3 = 10^{-7}$ );
- optimality tolerance ( $\epsilon_4 = 10^{-6}$ ).

In Fig. 1 is depicted a flow chart scheme representing the essential structure of the simulation and optimization program.

#### 4. Experimental apparatus for thermal diffusivity measurements

In the present study an experimental apparatus for subjecting a solid specimen to a temperature gradient with variable time evolution has been developed. The system is well visualized in Fig. 2.

It consists of three main modules. The first consists of two Peltier cells with a nominal thermal power of 100 W. The Peltier cells are electrically powered by two control boards (the second module) that modulates the power intensity to be supplied to the Peltier cells. The electrical controllers are fully driven by an application (third module) developed in the Labview environment. The heating modules operate both as source and as sink for pumping and removing heat from the cold and hot side of the specimen. The lateral boundary surfaces are guarded by an insulating material, whose thermal conductivity is equal to  $0.034 \text{ [W/mK]}$  and the thickness is equal to  $8 \cdot 10^{-2} \text{ [m]}$ . The workable area surface of the heating modules is equal to  $230 \times 122 \cdot 10^{-6} \text{ [m}^2\text{]}$ .

Additional aluminum plates of 10 mm in thickness are integrated as a part of the main plate of the heating modules and they are equipped by four thermo-resistances sensors (PT 1000) of Class DIN, a maximum error of that is equal to  $0.08K$  at  $0 \text{ }^\circ\text{C}$ . The values of the temperature sensors are used as feedback signals for adjusting the thermal power according to the selected set point

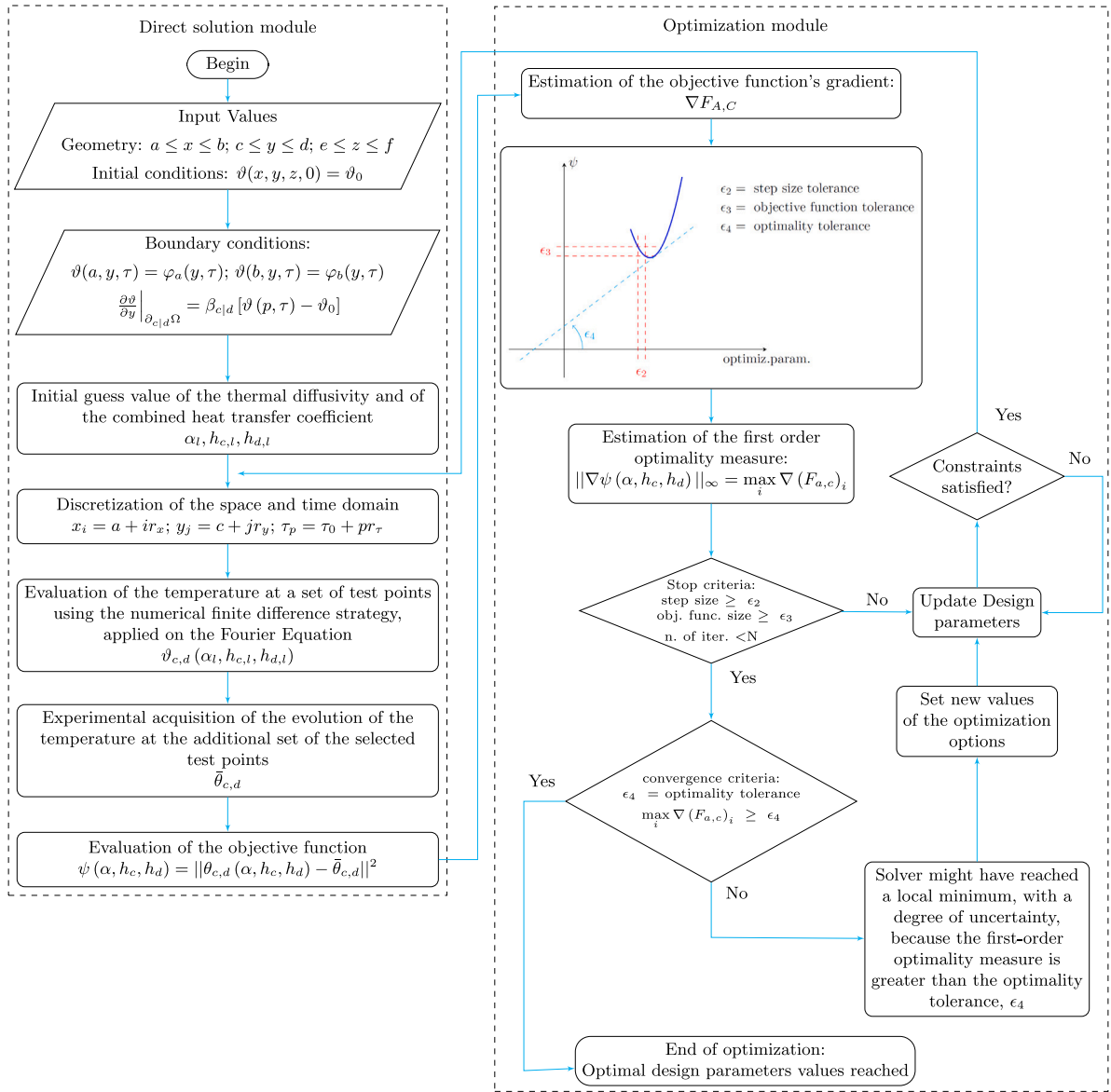


Fig. 1. Flow chart scheme representing the essential structure of the simulation and optimization program.

values on the cold and hot side. Another thermo-resistance PT1000 is placed outside the device in order to measure the surrounding ambient temperature, and the same temperature is used for the pre-test calibration of the thermocouple's sensor.

Moreover, two custom heat flux meters (HFMs), with a measuring area equal to  $230 \times 122 \cdot 10^{-6} \text{ [m}^2\text{]}$  and with a nominal sensitivity equal to 4.14 and  $4.04 \left[ \frac{\text{W}}{\text{m}^2\text{mV}} \right]$  are assembled side to side on the two aluminum plates. The other opposite sides of the HFMs are then arranged in direct contact with the two opposite faces of the specimen, for measuring the heat fluxes (HF) across them. The measures of the HF are then compared to each other, when the steady state regime is fully developed, in order to verify the unidirectional distribution throughout the specimen. The discrepancy between the two values of the HF is indicative of the heat losses across the lateral surfaces in steady state condition. The electrical signals provided by the two HFMs are acquired with a resolution of 24 bit, at a rate of 75 [Sample/s] and with a sensitivity of 0.02 °C. Since the acquisition system is limited by a maximum value of the input signal equal to 80 [mV], as a consequence of it, a heat flow value greater than  $\dot{q}_{\text{max}} = 331.2 \left[ \frac{\text{W}}{\text{m}^2} \right]$ , cannot be measurable. Considering the approximating assumption of a semi-infinite solid, whose boundary is subject to a constant heat power equal to  $\dot{q}_{\text{max}}$ , a limit value of the thermal diffusivity-time product coefficient arises from the following inequality

$$(\alpha \cdot \tau) \gtrsim \pi \left[ \frac{(\theta_{\text{sp}} - \theta'_0) k}{2\dot{q}_{\text{max}}} \right]^2 \tag{4.1}$$

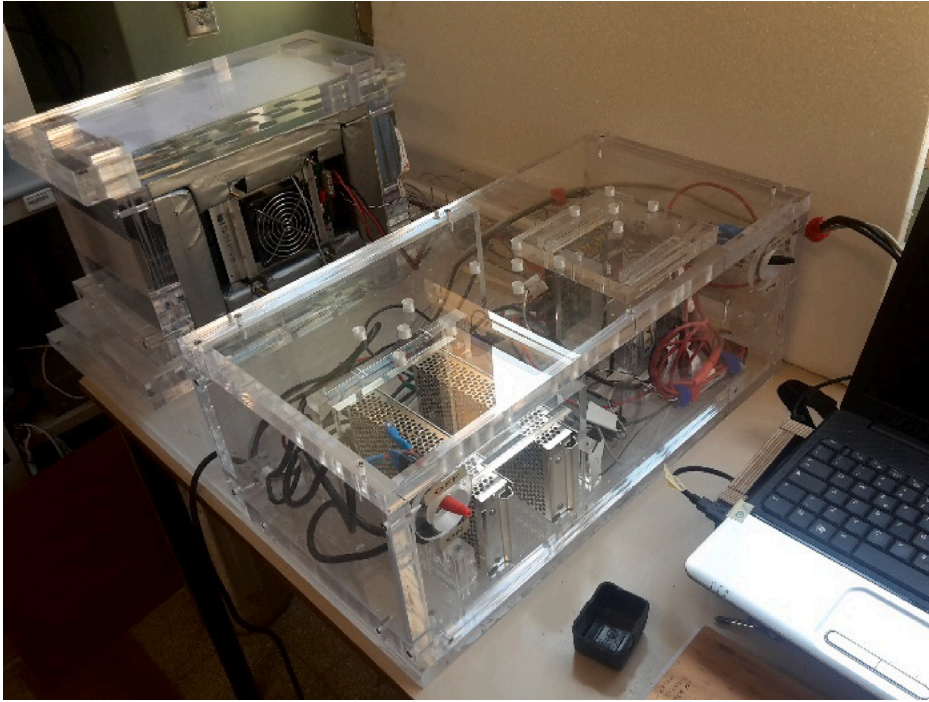


Fig. 2. Experimental Apparatus for thermal diffusivity measurement.

where  $\vartheta_{sp}$  is the value of the temperature assumed as set point at the boundary,  $\tau$  is the instant at which the temperature at the boundary achieves the  $\vartheta_{sp}$  value.

Four additional T thermocouple sensors are incorporated inside the HFMs. Two of them acquire the absolute surface's temperature of the specimen, while the others two are connected in differential configuration for measuring directly the temperature difference among the specimen, in order to reduce the error.

During the experiment the sample is sandwiched in between the two HFMs and the whole system are hold tightly together, by means of a self-made screwing clamp system for ensuring a good thermal contact; see Fig. 4.

The following scheme for modeling the lateral heat losses has been developed and implemented in the optimization model.

The heat exchanges between the lateral surfaces and the surrounding environment can be locally expressed as:

$$-k \frac{\partial \vartheta}{\partial y} \Big|_{y=c} = h_c [\vartheta'_c(x, \tau) - \vartheta'_0] \quad \text{and} \quad -k \frac{\partial \vartheta}{\partial y} \Big|_{y=d} = h_d [\vartheta'_d(x, \tau) - \vartheta'_0] \quad (4.2)$$

according to whether the heat flux across the lateral surface  $y = c$  or  $y = d$  is considered.

$\vartheta(x, \tau)$  represents the temperature distribution on the lateral surfaces. Since measuring the temperatures at each point  $x = x_i$  might be quite difficult, a first order approximation can be considered in place of them:

$$\begin{cases} \vartheta_c(x, \tau) \\ \vartheta_d(x, \tau) \end{cases} \cong \vartheta^{(0)}(x_i) = \frac{\vartheta(a, \tau) - \vartheta(b, \tau)}{b - a} x_i + \frac{a\vartheta(b, \tau) - b\vartheta(a, \tau)}{b - a}.$$

In Fig. 3 the spatial distribution of the temperature on a lateral surface of the specimen is schematically represented. It is worthwhile noting that, even if  $\vartheta_c(x, \tau)$  and  $\vartheta_d(x, \tau)$  could be in general different, however the first order approximations of them, for symmetry reasons, have the same value  $\vartheta^{(0)}$ . Moreover, the combined heat transfer coefficients  $h$  should hold their different subscripts for reminding us that they could have different values, because the surrounding environment could have a not uniform bearing on the specimen.

## 5. Experimental results

In the present study a preliminary experimental investigation for evaluating the behavior of the developed apparatus has been carried out on a specimen made of poly methyl methacrylate (PMMA). This material represents an acceptable approximation of the assumptions mentioned in the previous paragraph. This material is also attractive because the scientific literature collects many studies in which the thermal diffusivity is delivered within a restricted range of values. Rohde et al. in [46] have performed an inter

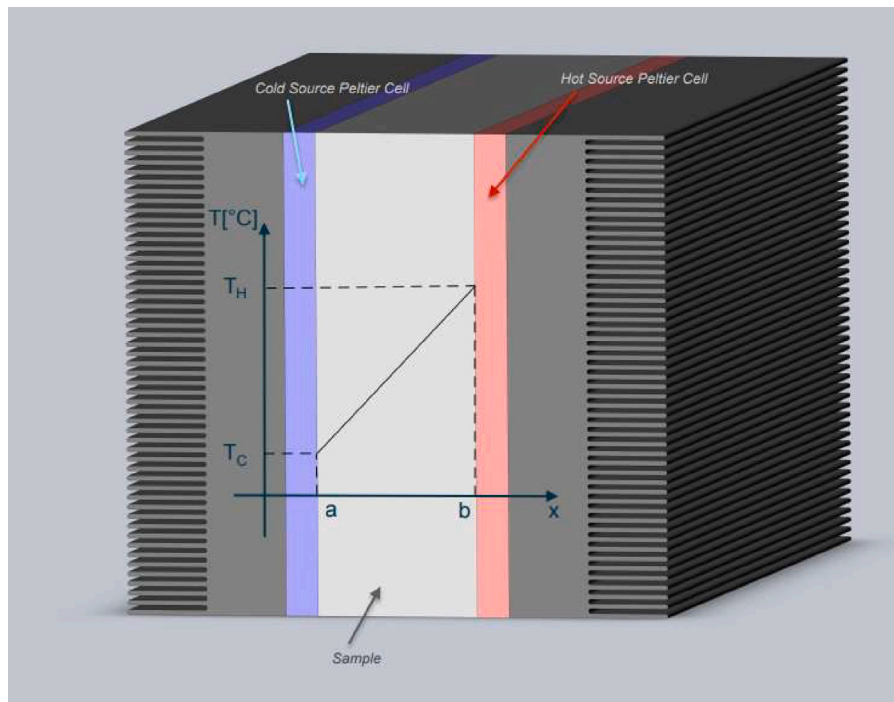


Fig. 3. First order approximation of the spatial distribution of the temperature on the lateral surface.

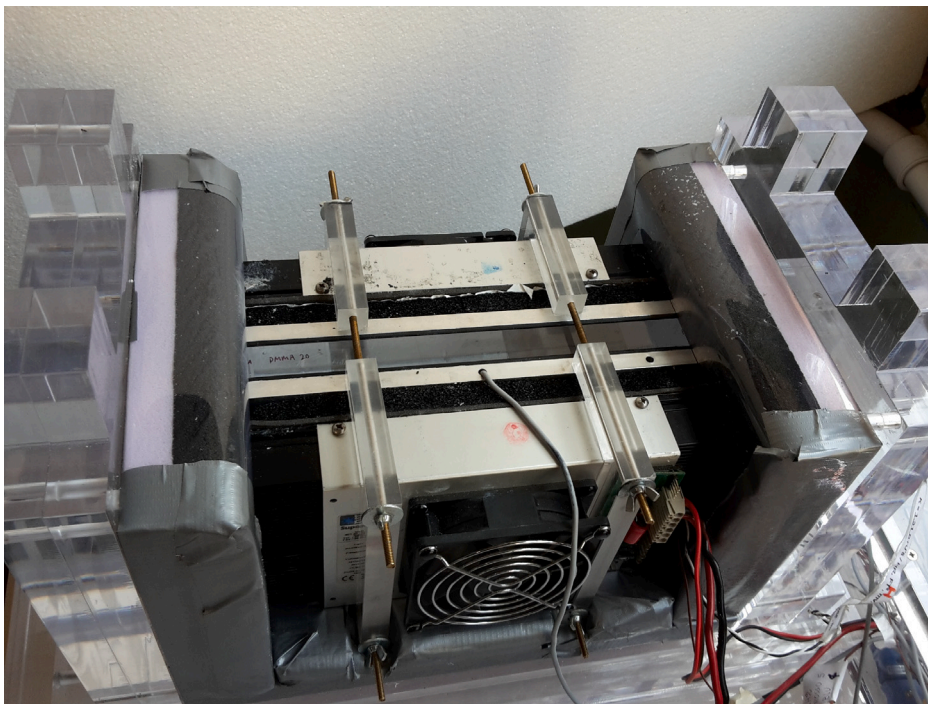


Fig. 4. Specimen of PMMA under test, sandwiched between the Peltier cells by means of the screwing clamp system for ensuring a good thermal contact.

laboratory comparison on the measured values of the thermal diffusivity of a PMMA specimen. Eleven independent and blinded certificated laboratories have obtained different values for  $\alpha$  at room temperature, settled between  $[20 \div 40]$  °C. The range over

**Table 1**  
Reference values of the PMMA material at 25 °C reported in [46].

Density	Diffusivity	Conductivity
1188 kg/m <sup>3</sup>	0.113 mm <sup>2</sup> /s	0.193 W/mK

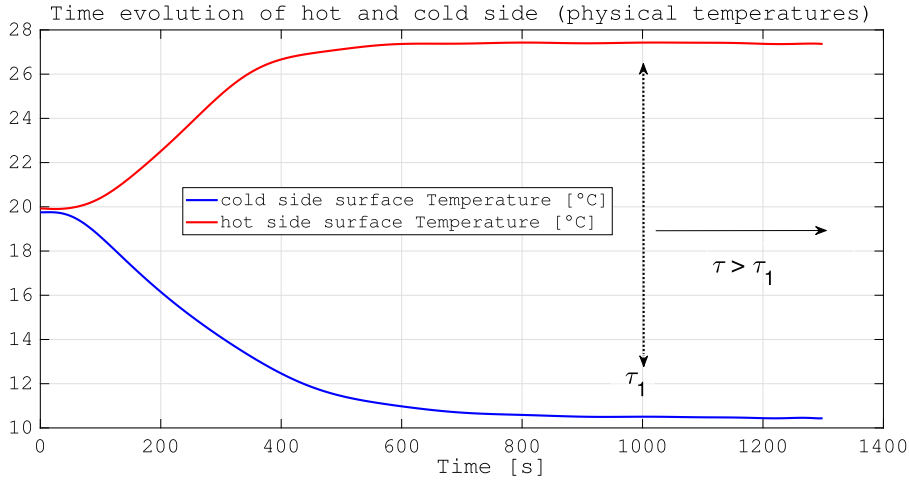


Fig. 5. Time evolution of the surface temperature at the hot and cold side of the specimen. (For interpretation of the references to color in this figure legend, the reader is referred to the web version of this article.)

which the measured values of  $\alpha$  fall is restricted to a maximum and minimum value, respectively equal to

$$\alpha_{\max} = 0.13 \cdot 10^{-6} \left[ \frac{\text{m}^2}{\text{s}} \right] \quad \text{and} \quad \alpha_{\min} = 0.095 \cdot 10^{-6} \left[ \frac{\text{m}^2}{\text{s}} \right]$$

and the average value is equal to

$$\alpha_{\text{ave}} \approx 0.113 \cdot 10^{-6} \left[ \frac{\text{m}^2}{\text{s}} \right].$$

In Table 1 are reported the characteristic values to which we can refer for PMMA material at 25 °C [46].

The specimen of PMMA has been arranged inside the main module of the system as illustrated in Fig. 4, where it appears sandwiched between two aluminum plates and clumped by a screwing system.

All the thermocouple sensors are initially calibrated, and the environment temperature is used as initial condition of the specimen.

Once the two set points are adjusted 10 °C degrees above and below the ambient temperature, the specimen is then progressively heated and cooled.

In Fig. 5 are depicted the time evolutions of the temperatures at both sides of the specimen when the heating and cooling modules respectively operate as source and as sink of heat. The evolution spans from the initial conditions, exhibiting a transient behavior, up to the achievement of the steady state conditions. The instant for which the transient regime can be considered extinguished is remarked with the label  $\tau_1$ . For  $\tau > \tau_1$ , the heat flux and the temperatures on the opposite sides of the specimen can be approximated to a constant value since their running average values exhibits small temporal variations, the deviations ranging from 0.5% to 1%. The following observations warrant consideration since explain why the representation provided in Fig. 5 is extended up to including the steady regime, despite the experimental data occurred after  $\tau_1$  are not suitable for estimating the thermal diffusivity. It should be noted that the mathematical scheme, expressed by the combination of Eqs. (3.6) and (3.7), involves the parameters  $\beta_c$  and  $\beta_d$ , that denote the ratio of the heat transfer coefficients  $h_c$  and  $h_d$  over the thermal conductivity  $\lambda$  of the specimen. Therefore, the quantities that are directly subjected to optimization, in addition to  $\alpha$ , are in effect  $\beta_c$  and  $\beta_d$ . Consequently, the optimization procedure identifies the optimal values  $\beta_{c,\text{opt}}$  and  $\beta_{d,\text{opt}}$ , rather than the optimal values  $h_{c,\text{opt}}$  and  $h_{d,\text{opt}}$ . However, the optimal values of the heat transfer coefficients might be derived from  $\beta_{c,\text{opt}}$  and  $\beta_{d,\text{opt}}$  by using the following simple relations:

$$h_{d,\text{opt}} = [\lambda \cdot \beta]_{d,\text{opt}} \quad (5.1)$$

$$h_{c,\text{opt}} = [\lambda \cdot \beta]_{c,\text{opt}} \quad (5.2)$$

provided that the value of the thermal conductivity be a known quantity, eventually even derived from additional circumstances. Indeed, the unknown value of the thermal conductivity in the previous equations, can be then evaluated by using the heat flux and the temperatures extracted during a time interval where  $\tau$  is greater than  $\tau_1$ , and the quantities can be considered stationary.

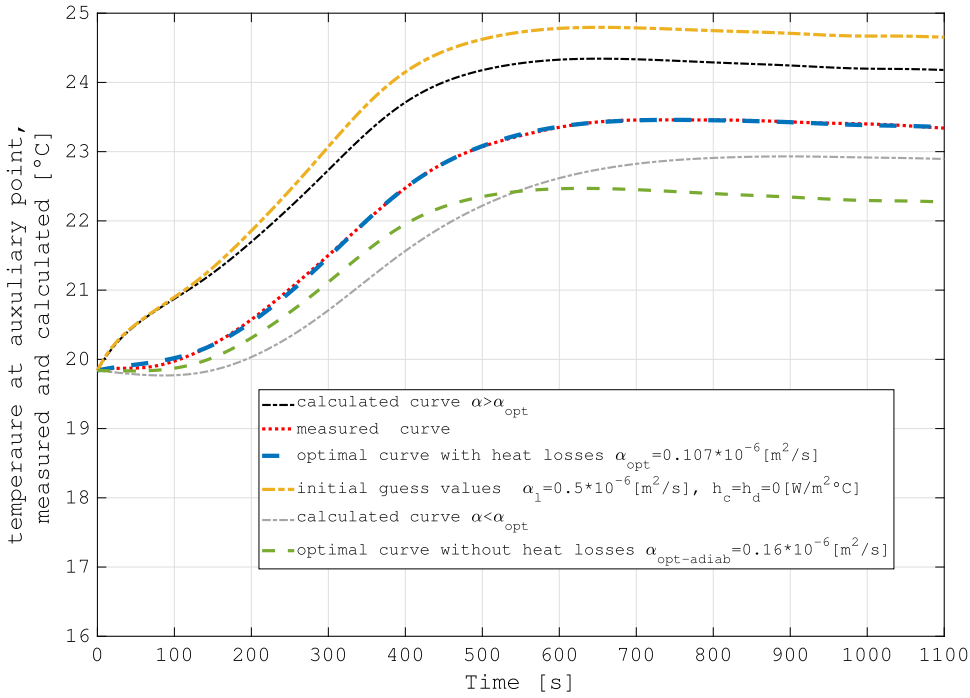


Fig. 6. Experimental and calculated time evolution curves of the temperature at the auxiliary point at the lateral surface. The vertical axis represents the measured and calculated temperature at auxiliary point.

In Fig. 6 is represented the experimental temperature measured at a selected auxiliary point  $P(\hat{x}, c)$ , belonging to the lateral surface at  $y = c$ . The experimental time profile is depicted with the red dot curve. The numerical resolution of Eqs. (3.7) and (3.10) provides a simulated temperature at the same point  $P$ , when numerical values of  $\alpha$ ,  $h_c$  and  $h_d$  are a priori assigned.

In Fig. 6, examples of calculated temperature time profiles are depicted with different colors and styles (dash-dot orange, black, blue, gray and green). The orange curve corresponds to an initial assignment of the guess values of the optimization parameters equal to:

$$\alpha_l = 0.5 \cdot 10^{-6} \left[ \frac{\text{m}^2}{\text{s}} \right], \quad h_c = h_d = 0 \left[ \frac{\text{W}}{\text{m}^2\text{K}} \right]$$

(that corresponds to an ideal adiabatic guard section). Only the optimal values of  $\alpha$ ,  $h_c$  and  $h_d$  provide a calculated curve overlapped to the experimental data (depicted with the red dotted curve). The blue curve represents the optimal calculated temporal profile that minimize the error function of Eq. (3.7). The optimal values of the explanatory parameters are equal to:

$$\alpha_{\text{opt}} = 0.107 \cdot 10^{-6} \left[ \frac{\text{m}^2}{\text{s}} \right], \quad h_{c,\text{opt}} = 0.4 \left[ \frac{\text{W}}{\text{m}^2\text{K}} \right] \quad \text{and} \quad h_{d,\text{opt}} = 0.45 \left[ \frac{\text{W}}{\text{m}^2\text{K}} \right].$$

The difference between the optimal calculated value of the thermal diffusivity and the reference value, indicated in Table 1, is lower than 5%

$$100 \frac{|\alpha_{\text{ref}} - \alpha_{\text{opt}}|}{\alpha_{\text{ref}}} < 5\%. \tag{5.3}$$

The green dash-dot curve corresponds to the optimal profile when the heat loss correction factors are neglected, therefore an ideal adiabaticity at lateral surfaces is assumed. The discrepancy with respect to the experimental curve is significantly greater than the previous curve that incorporates the heat losses. The corresponding error is lower than 34

$$100 \frac{|\alpha_{\text{ref}} - \alpha_{\text{opt-adiab}}|}{\alpha_{\text{ref}}} < 34\%. \tag{5.4}$$

## 6. Conclusion and further developments

In the present research study, an optimization technique, coupled with an experimental apparatus, for determining the thermal diffusivity of solid materials, has been devised and experimentally validated. The solving approach belongs to a class of direct solution methods in which the solution of the inverse problem of the heat equation in transient conditions is numerically supervised

by an optimization model. Modeling the heat losses, caused by the imperfect adiabaticity at the insulated sides of the specimen, with auxiliary Robin conditions has proved an effective strategy for significantly improving the estimation of the thermal diffusivity. The devised technique makes use of a low-cost apparatus for generating a suitable thermal field and extracting the experimental data while the test of the specimen is in progress. The measurement apparatus has been tested on a specimen made of PMMA since it can be considered an acceptable approximation of the isotropic, homogeneous conduction model to which the classical Fourier equation is founded. The following conclusions can be drawn from the present experimental investigation on thermal diffusivity measurements of a solid material.

1. The optimization procedure developed identifies an optimal value of the thermal diffusivity that changes according to whether the heat losses are taken or not into account.
2. Incorporating the heat loss correction in the solution of the heat equation significantly improves the estimation of the thermal diffusivity value.
3. The estimated thermal diffusivity is in good agreement with the measured values delivered by an experimental investigation [46] consisting in an inter-laboratory comparison of eleven laboratory equipped with Laser Flash, hot disk and hot bridge apparatus. The error between the optimal value and the reference average value of  $\alpha_{\text{ref}}$  delivered by an inter-laboratory comparison of eleven certified measurements turns out to be lower than 5%. The experimental profile of the surface temperature broadly matches the simulated curves generated by the model.
4. The observed results reveal a reliable capability of the model to identify the thermal diffusivity value that explain the relation among the functional dependence underlying the experimental observations.
5. The obtained results are quite reasonable considering the low-cost equipment used in this study.

The study constitutes a valuable contribution for those that are involved in classical heat transfer concepts under transient conditions. Specifically, incorporating the heat transfer coefficients into a global optimization procedure, simultaneously with the thermal diffusivity value, deserve consideration.

The obtained results can be considered satisfactory considering that the model is based on the approximating assumption of the 2D formalism. The accuracy could be susceptible to further improvements if the optimization is performed globally over an error function in which more than one additional surface temperatures and/or heat fluxes are accounted for. This exploratory investigation suggests that it could be convenient and fruitful to perform further refinement of the research by extending the numerical inversion of the heat equation to a 3D formalism for characterizing non-homogeneous media. Moreover, the uniqueness of the optimal solution, over the domain of the explanatory variables ( $\alpha$ ,  $h_c$ ,  $h_d$ ), deserves consideration for future investigations.

### Declaration of competing interest

The authors declare that they have no known competing financial interests or personal relationships that could have appeared to influence the work reported in this paper.

### Data availability

Data will be made available on request.

### Acknowledgments

The funding Agency Thanks to Sotacarbo SpA Sustainable Energy Research Centre (The funding Agency did not play any role in the conceptualization, design, and execution of the research) Grant number: I12F17000070001.

### References

- [1] R. Baccoli, C. Mastino, G. Rodriguez, Energy and exergy analysis of a geothermal heat pump air conditioning system, *Appl. Therm. Eng.* 86 (2015) 333–347.
- [2] M. Khoukhi, S. Abdelbaqi, A. Hassan, Transient temperature change within a wall embedded insulation with variable thermal conductivity, *Case Stud. Therm. Eng.* 20 (2020) 100645.
- [3] A. Karaki, M. Mohammad, E. Masad, M. Khraisheh, Theoretical and computational modeling of thermal properties of lightweight concrete, *Case Stud. Therm. Eng.* 28 (2021) 101683.
- [4] Á. Lakatos, A. Csík, I. Csarnovics, Experimental verification of thermal properties of the aerogel blanket, *Case Stud. Therm. Eng.* 25 (2021) 100966.
- [5] M. Khoukhi, S. Abdelbaqi, A. Hassan, A. Darsaleh, Impact of dynamic thermal conductivity change of EPS insulation on temperature variation through a wall assembly, *Case Stud. Therm. Eng.* 25 (2021) 100917.
- [6] H.S. Carslaw, J.C. Jaeger, 2nd Ed., Clarendon Press, Oxford, 1959, 1959.
- [7] A. Salazar, On thermal diffusivity, *Eur. J. Phys.* 24 (4) (2003) 351–358.
- [8] R. Brito, S. Carvalho, S.L.E. Silva, Experimental investigation of thermal aspects in a cutting tool using comsol and inverse problem, *Appl. Therm. Eng.* 86 (2015) 60–68.
- [9] W.J. Parker, R.J. Jenkins, C.P. Butler, G.L. Abbott, Flash method of determining thermal diffusivity, heat capacity, and thermal conductivity, *J. Appl. Phys.* 32 (9) (1961) 1679–1684.
- [10] N. Sparvieri, E. Penco, C. Sibilia, M. Bertolotti, G. Suber, A. Ferrari, A laser interferometric method applied to thermal diffusivity measurements of ferrites, *Mater. Lett.* 5 (11–12) (1987) 449–452.
- [11] A. Mandelis (Ed.), *Progress in Photothermal and Photoacoustic Science and Technology*, Vol. II, Prentice-Hall, Englewood Cliffs, NJ, 1994.

- [12] B. Dongmei, C. Huanxin, L. Shanjian, S. Limei, Measurement of thermal diffusivity/thermal contact resistance using laser photothermal method at cryogenic temperatures, *Appl. Therm. Eng.* 111 (2017) 768–775.
- [13] L. Vozár, W. Hohenauer, Uncertainty of thermal diffusivity measurements using the laser flash method, *Int. J. Thermophys.* 26 (6) (2005) 1899–1915.
- [14] B. Hay, J. Filtz, J. Hameury, L. Rongione, Uncertainty of thermal diffusivity measurements by laser flash method, *Int. J. Thermophys.* 26 (6) (2005) 1883–1898.
- [15] M.J. Assael, K.D. Antoniadis, W.A. Wakeham, Historical evolution of the transient hot-wire technique, *Int. J. Thermophys.* 31 (6) (2010) 1051–1072.
- [16] J.J. Healy, J.J. De Groot, J. Kestin, The theory of the transient hot-wire method for measuring thermal conductivity, *Physica B+ C* 82 (2) (1976) 392–408.
- [17] L. Vozár, A computer-controlled apparatus for thermal conductivity measurement by the transient hot wire method, *J. Therm. Anal.* 46 (2) (1996) 495–505.
- [18] J. Fan, H. Mu, C. Gao, F. Song, High pressure thermal conductivity of three ethyl esters in the liquid phase, *Case Stud. Therm. Eng.* 27 (2021) 101235.
- [19] Y. Nagasaka, A. Nagashima, Simultaneous measurement of the thermal conductivity and the thermal diffusivity of liquids by the transient hot-wire method, *Rev. Sci. Instrum.* 52 (2) (1981) 229–232.
- [20] W.N.D. Santos, R. Gregorio Jr., Hot-wire parallel technique: A new method for simultaneous determination of thermal properties of polymers, *J. Appl. Polym. Sci.* 85 (8) (2002) 1779–1786.
- [21] X. Zhang, M. Fujii, Measurements of the thermal conductivity and thermal diffusivity of polymers, *Polym. Eng. Sci.* 43 (11) (2003) 1755–1764.
- [22] G.C. Glatzmaier, W.F. Ramirez, Simultaneous measurement of the thermal conductivity and thermal diffusivity of unconsolidated materials by the transient hot wire method, *Rev. Sci. Instrum.* 56 (7) (1985) 1394–1398.
- [23] S.E. Gustafsson, Transient plane source techniques for thermal conductivity and thermal diffusivity measurements of solid materials, *Rev. Sci. Instrum.* 62 (3) (1991) 797–804.
- [24] Y. He, Rapid thermal conductivity measurement with a hot disk sensor: Part 1. theoretical considerations, *Thermochim. Acta* 436 (1–2) (2005) 122–129.
- [25] E. García, I. Amaya, R. Correa, Estimation of thermal properties of a solid sample during a microwave heating process, *Appl. Therm. Eng.* 129 (2018) 587–595.
- [26] C. Fabiani, A. Pisello, Coupling controlled environmental forcing and transient plane source method: An innovative thermal characterization procedure for building insulation materials, *Appl. Therm. Eng.* 130 (2018) 254–263.
- [27] C. Huang, W.-K. Lin, J.-K. Chen, Important factors affecting the thermal resistance and thermal diffusivity of vapor chambers, *Appl. Therm. Eng.* 126 (2017) 1148–1155.
- [28] H. Naseem, H. Murthy, A simple thermal diffusivity measurement technique for polymers and particulate composites, *Int. J. Heat Mass Transfer* 137 (2019) 968–978.
- [29] M.N. Ozisik, *Inverse Heat Transfer: Fundamentals and Applications*, CRC Press, 2000.
- [30] O.M. Alifanov, *Inverse Heat Transfer Problems*, Springer Science & Business Media, 2012.
- [31] M. Monde, Y. Mitsutake, A new estimation method of thermal diffusivity using analytical inverse solution for one-dimensional heat conduction, *Int. J. Heat Mass Transfer* 44 (16) (2001) 3169–3177.
- [32] P.L. Woodfield, M. Monde, Y. Mitsutake, On estimating thermal diffusivity using analytical inverse solution for unsteady one-dimensional heat conduction, *Int. J. Heat Mass Transfer* 50 (5–6) (2007) 1202–1205.
- [33] M. Monde, M. Kosaka, Y. Mitsutake, Simple measurement of thermal diffusivity and thermal conductivity using inverse solution for one-dimensional heat conduction, *Int. J. Heat Mass Transfer* 53 (23–24) (2010) 5343–5349.
- [34] N. Ukrainczyk, Thermal diffusivity estimation using numerical inverse solution for 1d heat conduction, *Int. J. Heat Mass Transfer* 52 (25–26) (2009) 5675–5681.
- [35] X.T. Xiong, W.X. Shi, Y.C. Hon, A one-dimensional inverse problem in composite materials: Regularization and error estimates, *Appl. Math. Model.* 39 (18) (2015) 5480–5494.
- [36] Y.-C. Hua, T. Zhao, Z.-Y. Guo, Optimization of the one-dimensional transient heat conduction problems using extended entransy analyses, *Int. J. Heat Mass Transfer* 116 (2018) 166–172.
- [37] J.M. Laskar, S. Bagavathiappan, M. Sardar, T. Jayakumar, J. Philip, B. Raj, Measurement of thermal diffusivity of solids using infrared thermography, *Mater. Lett.* 62 (17–18) (2008) 2740–2742.
- [38] W.-Z. Fang, J.-J. Gou, L. Chen, W.-Q. Tao, A multi-block lattice Boltzmann method for the thermal contact resistance at the interface of two solids, *Appl. Therm. Eng.* 138 (2018) 122–132.
- [39] A.L. Cottrill, R. Goulet, F. Fremy, J. Meulemans, M.R. Sheldon, M.Z. Bazant, Simultaneous inversion of optical and infra-red image data to determine thermo-mechanical properties of thermally conductive solid materials, *Int. J. Heat Mass Transfer* 163 (2020) 120445.
- [40] T. Zhou, R. zheng Fang, D. Jia, P. Yang, Z. ying Ren, H. bai Bai, Numerical and experimental evaluation for density-related thermal insulation capability of entangled porous metallic wire material, *Def. Technol.* (2022).
- [41] T. Salahuddin, M. Khan, T. Saeed, M. Ibrahim, Y.-M. Chu, Induced MHD impact on exponentially varying viscosity of williamson fluid flow with variable conductivity and diffusivity, *Case Stud. Therm. Eng.* 25 (2021) 100895.
- [42] A. Salazar, M. Colom, A. Mendioroz, Laser-spot step-heating thermography to measure the thermal diffusivity of solids, *Int. J. Therm. Sci.* 170 (2021) 107124.
- [43] C. Ding, L. Wang, Z. Niu, Thermal performance evaluation of latent heat storage systems with plate fin-metal foam hybrid structure, *Case Stud. Therm. Eng.* 27 (2021) 101309.
- [44] U. Ali, K.J.B.A. Karim, N.A. Buang, A review of the properties and applications of poly (Methyl Methacrylate) (PMMA), *Polym. Rev.* 55 (4) (2015) 678–705.
- [45] W. An, X. Yin, M. Cai, Y. Tang, Q. Li, X. Hu, Influence of U-shaped structure on upward flame spread and heat transfer behaviors of PMMA used in building thermal engineering, *Case Stud. Therm. Eng.* 22 (2020) 100794.
- [46] M. Rohde, F. Hemberger, T. Bauer, J. Blumm, T. Fend, T. Häusler, U. Hammerschmidt, W. Hohenauer, K. Jaenicke-Rössler, E. Kaschnitz, E. Pfaff, G. Pintsuk, Intercomparison of thermal diffusivity measurements on CuCrZr and PMMA, *High Temp.-High Press.* 42 (6) (2013) 469–474.